ADVANCED MATERIALS INTERFACES
Open Access
www.advmatinterfaces.de

Nanoscale Porosity of High Surface Area Gadolinium Oxide Nanofoam Obtained With Combustion Synthesis

*Roos M. de Boer, Xiaodan Chen, Daniel Cvejn, Kateřina Peterek Dědková, Marijn A. van Huis, and Rafael G. Mendes**

Nanoscale gadolinium oxide (Gd_2O_3) is a promising nanomaterial with unique physicochemical properties that finds various applications ranging from biomedicine to catalysis. The preparation of highly porous Gd_2O_3 nanofoam greatly increases its surface area thereby boosting its potential for functional use in applications such as water purification processes and in catalytic applications. By using the combustion synthesis method, a strong exothermic redox reaction between gadolinium nitrate hexahydrate and glycine causes the formation of crystalline nanoporous Gd_2O_3. In this study, the synthesis of Gd_2O_3 nanofoam is achieved with combustion synthesis at large scale (grams). Its nanoscale porosity is investigated by nitrogen physisorption and its nanoscale 3D structure by electron tomography, and the formation process is investigated as well by means of in situ heating inside the transmission electron microscope. The bulk nanofoam product is highly crystalline and porous with a surface area of 67 m^2 g^{-1} as measured by physisorption, in good agreement with the electron tomographic 3D reconstructions showing an intricate interconnected pore network with pore sizes varying from 2 to 3 nm to tens of nanometers. In situ heating experiments point to many possibilities for tuning the porosity of the Gd_2O_3 nanofoam by varying the experimental synthesis conditions.

1. Introduction

The main added-value of nanomaterials in the majority of their applications is their large specific surface area. This proves beneficial for catalytic processes, adsorption of pollutants during water purification, as well as other fields of their implementation. Increasing the specific surface area is therefore an obvious pathway to increase the efficiency of materials used in these processes and technologies. This way, less material is needed making particular technology more cost-effective and sustainable. An effective way of increasing the surface area of a material is by making its structure porous. An example of such porous materials are nanofoams, which can be made with all kinds of materials including metals and metal oxides.[1]

Gadolinium is a lanthanide with a partially filled 4f shell, giving it unique optical as well as magnetic properties. It is also known to have a large thermal-neutron capture cross-section which is exploited in various applications.[2,3] At room temperature, gadolinium(III) oxide (Gd_2O_3) has a cubic crystal structure with space group $la\overline{3}$. Above 1200 °C, the monoclinic structure (space group C2/m) takes over as being the most stable structure, and also a hexagonal phase (space group $P\overline{4}m2$) exists at temperatures above 2100 °C.[4] Nanoscale Gd_2O_3 can be applied in, among others, sensing applications,[5,6] in catalysis for the improvement of sulfur cathode materials for lithium-ion batteries,[7,8] and in the treatment of contaminated water.[9–11] For the latter,

R. M. de Boer, X. Chen, M. A. van Huis, R. G. Mendes
Soft Condensed Matter
Debye Institute for Nanomaterials Science
Utrecht University
Princetonplein 5, Utrecht 3584 CC, The Netherlands
E-mail: r.g.mendes@uu.nl

D. Cvejn
ENET Centre
CEET
VŠB – Technical University of Ostrava
17. listopadu 15, Ostrava 708 33, Czech Republic

The ORCID identification number(s) for the author(s) of this article can be found under https://doi.org/10.1002/admi.202300060.

DOI: 10.1002/admi.202300060

K. Peterek Dědková
Centre for Advanced Innovation Technologies
VŠB – Technical University of Ostrava
17. listopadu 15, Ostrava 708 33, Czech Republic

K. Peterek Dědková
Department of Mining Engineering and Safety
Faculty of Mining and Geology
VŠB – Technical University of Ostrava
17. listopadu 15, Ostrava 708 33, Czech Republic

M. A. van Huis, R. G. Mendes
Electron Microscopy Centre
Utrecht University
Universiteitsweg 99, Utrecht 3584 CG, The Netherlands

it was found that porous Gd_2O_3 could be used for the treatment of nuclear waste water, where it could adsorb 1350.2 mg g^{-1} uranyl in aqueous solutions.[9] However, a metal organic framework template was used to introduce the porosity, which complicates the synthesis.

There are various methods available to synthesize nanoscale Gd_2O_3, which includes solid-state,[12] sol–gel,[13,14] hydrothermal,[15,16] and gel-combustion syntheses.[12,17] The focus of this paper is the gel-combustion synthesis of Gd_2O_3. The gel-combustion synthesis consists of mixing a metal precursor containing the oxidizer (typically nitrate anions) and a fuel (typically glycine) into a gel. Upon heating of the said gel, a strong exothermic reaction takes place, where the metal precursor oxidizes the fuel. During this reaction, the fuel and the oxidizer are transformed into oxidic waste products (typically gaseous) and nanostructured metal oxide crystals. The overproduction of gases during the reaction is a cause of highly porous nature of final metal oxides and formed materials can be classified as a nanofoam.[18] In the case of Gd_2O_3, gadolinium nitrate hexahydrate ($Gd(NO_3)_3 \cdot 6H_2O$) can be used as the metal precursor and glycine (NH_2CH_2COOH) as the fuel. This results in a porous crystalline Gd_2O_3 structure[17] which can be achieved without the use of a template, thereby simplifying the production of Gd_2O_3 for various applications such as water treatment and catalysis that require large surface area materials. Moreover, gel-combustion synthesis requires lower temperatures than direct calcination methods, making it a more energy-efficient synthesis route. Therefore, it is of a great scientific and industrial interest to investigate the combustion synthesis of porous gadolinium oxides.

We would like to emphasize that the present study is a continuation of our previous work on the gel-combustion synthesis process, and the reader is referred to the previous publication for the thermal analysis of the reaction, as well as the antibacterial properties of the synthesized Gd_2O_3 nanofoam.[17] This work shows the interesting structure of easy-to-synthesize Gd_2O_3 nanofoam, which combines the useful properties of gadolinium in a porous structure with an accessible surface and an energy-efficient synthesis route. In this study, the gel-combustion synthesis of Gd_2O_3 nanofoam was investigated in two main steps. First, the product from the large scale combustion synthesis was characterized by physisorption and electron tomography (ET) to determine the size distribution and nature of the pores. Physisorption is the scientific standard for measuring the surface area of a porous material. With ET, a 3D model of the material was reconstructed allowing the inspection of the inner pore structure. Second, in situ heating transmission electron microscopy (TEM) experiments of the gel were conducted as well. With the in situ setup, the sample can be heated inside the microscope, allowing for real time imaging during the synthesis. We provide a high-resolution 3D characterization of the morphological aspects of Gd_2O_3 nanofoam synthesized with combustion synthesis, while the in situ TEM investigations show further possibilities of this method to tune the porosity.

2. Results and Discussion

The initial transparent precursor solution composed of $Gd(NO_3)_3 \cdot 6H_2O$ and glycine is shown in **Figure 1**a. After the gel-combustion synthesis, the resulting material is a fine, white powder presented in Figure 1b. Detailed TEM investigations were conducted to obtain more information about the textural features of the Gd_2O_3 nanofoam. Figure 1c shows a single cylindrical piece of the nanofoam, showing a highly porous texture consisting of spherical pores with a wide size distribution. It can also be seen that the texture is presented as one whole and not composed of agglomerated particles as is often seen in combustion synthesis, and it is in apparent contradiction to previous findings on that particular material.[17] This could be caused by the relatively low temperature that is observed when glycine is used as fuel. A higher combustion temperature generally leads to a higher degree of agglomeration,[19] which can be obtained with different fuels.[18] The inset of Figure 1c shows a typical diffraction pattern (DP) of the material that can be indexed as cubic Gd_2O_3 as shown in Figure S1, Supporting Information. The very sharp rings also show that the material is crystalline. Inspection at larger magnification shows that the pores are bounded by nanocrystalline walls as shown in Figure 1d and vary in thickness from 4 to 10 nm. The nanofoam is crystalline as is clear from the DP in Figure 1c and from the high-resolution TEM (HRTEM) image presented in Figure 1e, and corresponds to the cubic phase of Gd_2O_3. The prepared Gd_2O_3 nanofoam is composed of different morphologies that vary from cylindrical and spherical (Figure S2a,b, Supporting Information) to irregular (Figure S2c, Supporting Information) textures as can be seen in the Supporting Information. The energy dispersive X-ray spectroscopy (EDS) mapping of the material presented in Figure S3, Supporting Information, shows the presence of Gd and O, and absence of N, indicating the successful conversion of the $Gd(NO_3)_3$ and the absence of precursor contaminations. The combustion synthesis of the gadolinium gel therefore yields highly crystalline but porous Gd_2O_3.

The Gd_2O_3 sample was analyzed using N_2 physisorption. The isotherm and pore size distribution can be seen in **Figure 2**. The desorption branch in the isotherm is slightly below the adsorption branch, indicating that the sample was not completely degassed. The surface area S_{BET} was determined to be 67 m^2 g^{-1} for this sample, which is high compared to other combustion synthesized nanofoams of similar composition using glycine as fuel (e. g. 10–34 m^2 g^{-1} in CeO_2, up to 7 m^2 g^{-1} in Gd_2O_3-Y_2O_3:Ce, and 5–25 m^2 g^{-1} in Lu_2O_3:Eu^{3+}).[20–23] Although other methods could achieve a higher surface area (e. g. 287, 98 m^2 g^{-1}),[24,25] these methods used templates to introduce the porosity. The combustion method is simpler and does not require any form of templating. Moreover, the pore structure is unique and interconnected, as will be discussed further below. With the value for the surface area, we can determine what the Sauter diameter of spherical particles would be if the surface of the spherical particles is the only contribution to the total surface area, which can be calculated according to:

$$d_{BET} = \frac{6}{\rho S_{BET}} \quad (1)$$

where ρ is the density of bulk Gd_2O_3, which is 7.41×10^6 g m^{-3}.[26] This gives a value of 12 nm for the Sauter diameter, which corresponds well with the 10 nm crystallite size that was determined with the Scherrer formula

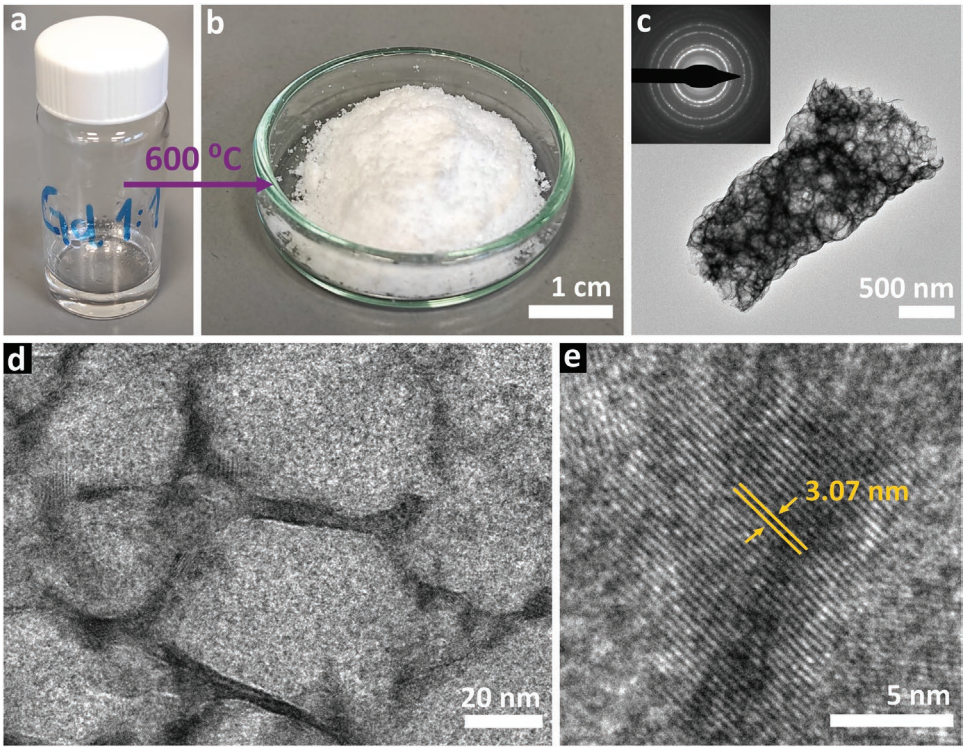

Figure 1. a,b) Photographs showing the precursor Gd gel (a) and the resulting Gd_2O_3 powder after heating (b). c–e) TEM images at different magnifications; (c) Bright-field TEM image of a grain of material from (b); the inset shows the corresponding electron DP, indicating that the material is crystalline. (d) Higher magnification TEM image showing the pore walls. (e) HRTEM image where atomic lattice fringes also show the high crystallinity of the material.

from X-ray diffraction (XRD) measurements in our previous work on this material.[17] The ratio between the particle sizes derived from the S_{BET} and from the XRD measurements gives an indication of the degree of agglomeration of the particles. The low ratio of 1.2 in this case supports the TEM observation that the material in fact does not consist of agglomerated particles. The Barrett–Joyner–Halenda (BJH) analysis shows that there is a narrow distribution of pores around 2 nm, a

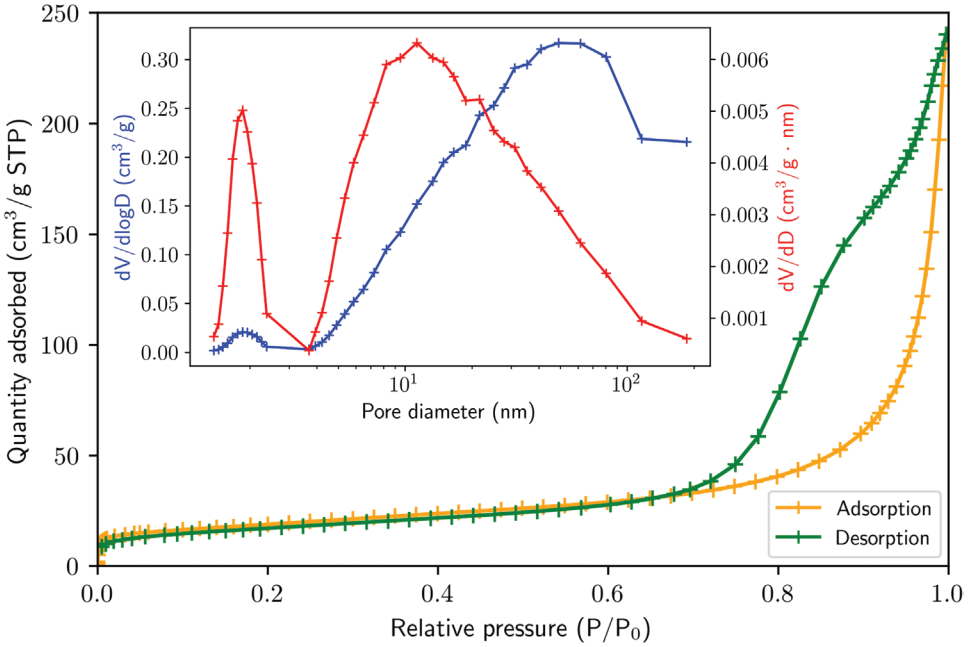

Figure 2. N_2 physisorption isotherms of the Gd_2O_3 with BJH pore size distributions derived from the adsorption branch shown in the inset.

ADVANCED MATERIALS INTERFACES
Open Access
www.advmatinterfaces.de

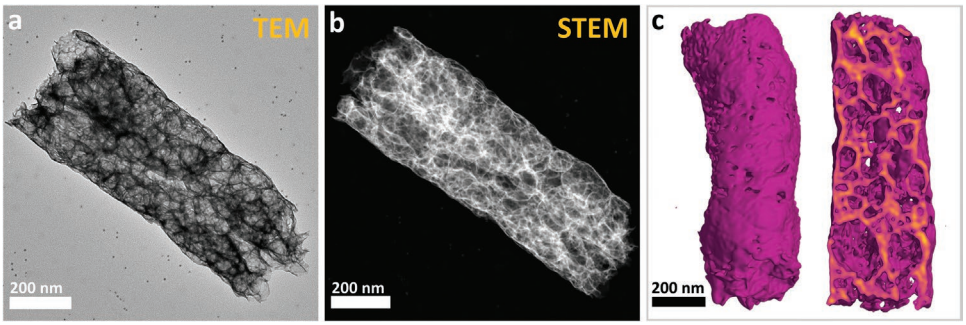

Figure 3. a) TEM and b) HAADF-STEM image of porous Gd_2O_3 obtained by combustion synthesis. The dots in the TEM image are gold nanoparticles, which are hardly visible in the STEM image because of the high contrast of the gadolinium. The surface and a cross-section of the corresponding 3D model reconstructed with tomography is shown in (c), showing surface pores and spherical inner pores.

distribution of mesopores around 10 nm, and a wide distribution of macropores. Although it is known that the BJH method underestimates the size of small mesopores due to the macroscopic assumptions in the Kelvin equation,[27] their presence can be indicated and is further investigated below with electron microscopy (see **Figures 3** and **4**). Furthermore, the BJH analysis also reveals a relatively negligible contribution of 2 nm pores to the total pore volume (Figure 2; blue line), presumably due to their small size. On the other hand, the same 2 nm pores do contribute significantly to the total surface area (Figure 2; red line), which means they are highly populated in the material. The presence of different pore sizes is probably related to the pore formation mechanism during the combustion synthesis. As the pores are formed from gas bubbles in the structure, there is likely a mechanism of coalescence and breaking of the gas bubbles causing the emergence of different pore size ranges. As combustion synthesis is a highly non-equilibrium process, it is very difficult to model this pore formation mechanism. Furthermore, the pore formation is dependent on (local) gas formation, temperature gradients, shear, and turbulent flow.

A tilt series of a typical larger piece of the Gd_2O_3 material was recorded with regular bright-field TEM and with high-angle annular dark field scanning TEM (HAADF-STEM); see Figure 3a,b, respectively. Experimental details can be found in the Experimental Section. From these tilt series, a 3D model of the material was reconstructed using tomography; see Figure 3c. Videos S1–S4, Supporting Information show the aligned tilt series, tomographic reconstruction, and 3D model. The tomographic reconstruction was made using the weighted back projection (WBP) algorithm because the simultaneous iterative reconstruction technique (SIRT)[28] was found to result in a worse reconstruction. The TEM and STEM recorded tilt series result in nearly identical 3D reconstructions. The 3D reconstructions shown in Figures 3 and 4 are all derived from the STEM tilt series.

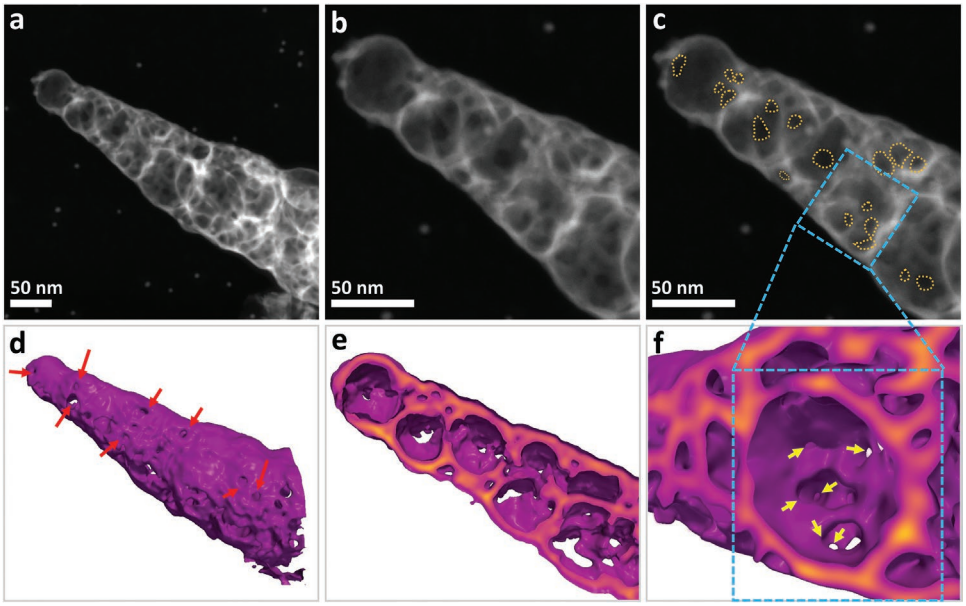

Figure 4. a–c) HAADF-STEM images of a small piece of porous Gd_2O_3 with corresponding tomographic reconstruction (d–f). The area indicated in (a) is enlarged in (b) and dark spots are highlighted in (c). The surface of the particle is shown in (d) with red arrows indicating pores in the wall of the particle. A cross-section of the reconstructed particle is shown in (e) and a magnified pore with smaller interconnecting pores indicated by yellow arrows can be seen in (f).

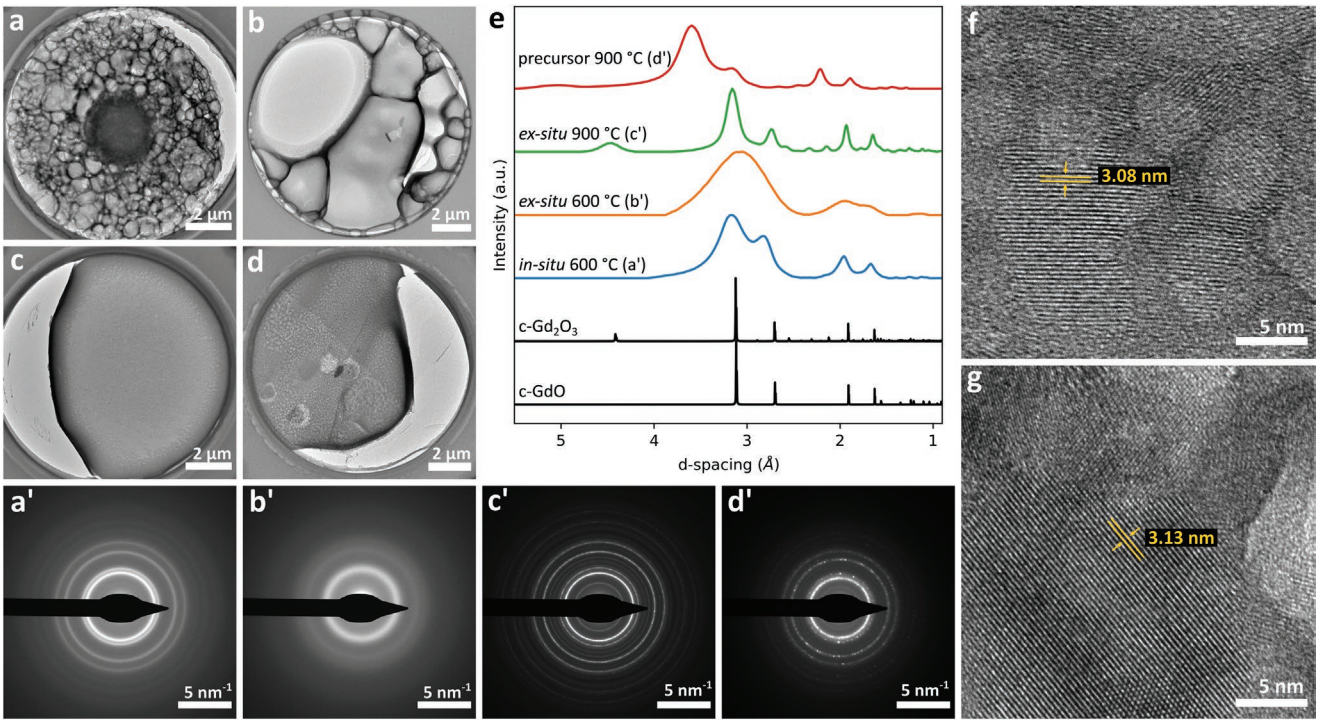

Figure 5. Overview of TEM images displaying typical viewing windows with GdO_x specimen on the heating chip recorded after a) in situ heating of the Gd gel to a temperature of 600 °C, b) ex situ heating of the Gd gel to 600 °C, c) ex situ heating of the Gd gel to 900 °C, d) in situ heating of the Gd precursor to 900 °C with corresponding DPs (a',b',c', and d', respectively), e) intensity profiles of the DPs and GdO and Gd_2O_3 phases, f) HRTEM images showing atomic lattices after heating in situ to 600 °C, and g) after heating ex situ to 900 °C. Indexed DPs can be seen in Figure S4, Supporting Information.

The surface of the 3D reconstruction (Figure 3c) shows pores on the surface of the material most probably formed during the emission of waste gases from the inside of the structure during the material-forming reactions. Figure 3c also shows the cross-section of the 3D reconstruction, where the complex inner pore structure of the material can be seen. The pores are mainly spherical, further suggesting their generation during the reaction, interconnected, and having a wide size distribution. Due to the low magnification that was used to image this larger piece of Gd_2O_3, there are less details that can be distinguished in the reconstruction. Therefore, a smaller piece was also analyzed, which was obtained after gently grinding the Gd_2O_3 powder. Figure 4 shows HAADF-STEM images and the tomographic reconstruction of the smaller Gd_2O_3 grain. The surface of the reconstructed volume shows pores in the wall of the material indicated by red arrows in Figure 4d. Owing to the higher magnification, it is now also possible to see smaller pores with sizes as small as 2 or 3 nm. Figure 4c highlights dark areas in the HAADF-STEM image that likely correspond to interconnections of pores within pore walls. The reconstructed cross-section of the area enclosed by the blue dashed lines is shown in Figure 4f, showing interconnecting pores depicted by the yellow arrows. From these results, we can infer that the Gd_2O_3 material made with combustion synthesis has an intricate network of interconnected pores with a wide size distribution. Videos of the aligned tilt series, tomographic reconstruction, and 3D model can be seen in the Videos S5–S7, Supporting Information.

In order to investigate the mechanism of the gel-combustion reaction more precisely, heating experiments were performed on the gel, where a small amount of gel was applied on a TEM heating chip and heated in situ (in the TEM column while imaged at every temperature) as well as ex situ (in ambient air without any intermediate imaging) for comparison. An overview of typical TEM observations seen during the heating experiments and the corresponding electron DPs can be seen in **Figure 5**.

The gel was first heated in situ to 600 °C with 100 °C increments. An overview of one of the windows on the heating chip (the windows are thin SiN_x membranes onto which the gel was applied) with a corresponding DP is shown in Figure 5a. The most prominent feature that stands out is the large scale porosity of the material. However, the DP (indexed in Figure S4, Supporting Information) indicates that here cubic GdO (space group $F\bar{4}3m$) has been formed and not the expected Gd_2O_3. From the images taken during the heating of the gel, it becomes apparent that the structures start to become porous from 100 °C onward; see Figure S5, Supporting Information. Besides the large scale porosity that can be seen in the overview of the window, the higher magnification images reveal that there is also small-scale porosity in the structure. From the HRTEM image in **Figure 6**a, it can be seen that there are small pores with a size of ≈2–3 nm, and bigger pores with a size ≈10–15 nm. This corresponds well with the pore size distribution that was obtained from N_2 physisorption on the bulk combustion sample. The high crystallinity of the material can also

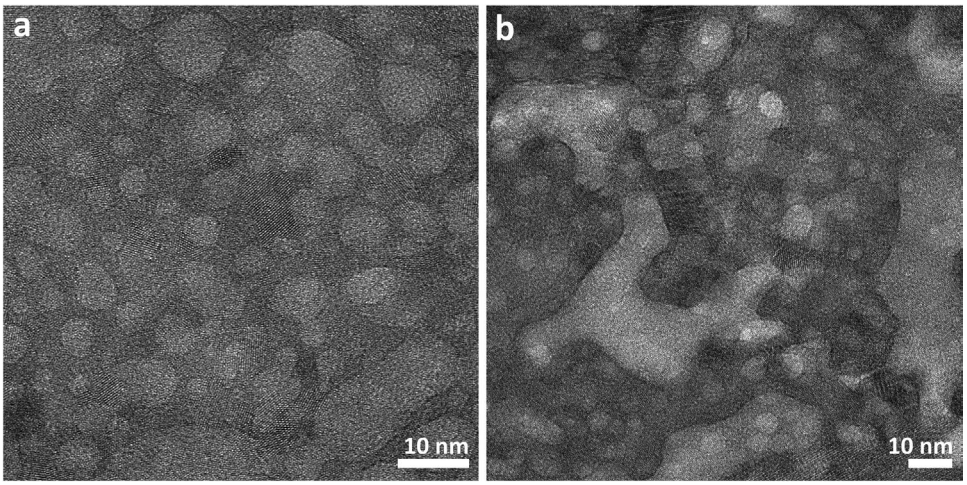

Figure 6. HRTEM images of the gadolinium gel when a) heated in situ to 600 °C and b) heated ex situ to 900 °C, showing small-scale porosity.

be seen from the lattice fringes that are present in the HRTEM image of Figure 5f. However, it was also observed that the electron beam could induce crystallization of the material. The HRTEM images may, therefore, not be representative for the rest of the material. From this in situ heating experiment, we can conclude that the material develops its porosity at low temperatures, and that the crystallization likely develops at higher temperatures or even during annealing after the combustion is complete. The formation of GdO instead of Gd_2O_3 could be caused by the lower temperature that is reached on this small-scale (exothermic heat from the reaction escapes more easily from the sample). Moreover, the vacuum conditions of the microscope limiting the accessibility of atmospheric oxygen for the reaction can also explain the lower oxidation degree of the resulting material. The sample was imaged again after 6 weeks and was found to have transformed into an amorphous state, and the porosity of the sample was lost; see Figure S6, Supporting Information. In this post-inspection experiment, the electron beam had a large effect on the amorphous sample, where short electron irradiation caused the structure to become porous again.

As it was hypothesized that the vacuum conditions in the TEM might prevent the oxidation of the gadolinium precursor to Gd_2O_3, the gel was also heated ex situ under atmospheric conditions. In the first ex situ experiment, the gel was heated to 600 °C such as in the in situ experiment. However, this resulted in an amorphous structure as can be seen in Figure 5b'. As such, the gel was heated to 900 °C in a second ex situ experiment. There, the succesful oxidation to Gd_2O_3 was indeed observed (Figure 5c'). Notably, this time, the characteristic large scale porosity seen in the in situ experiment was not observed. This could be caused by the absence of vacuum in the ex situ experiments. The smaller scale porosity; however, remained, which can be seen in the HRTEM image in Figure 6b. The crystallinity of the material, which was already indicated by the sharp rings in the DP, is also reflected in the lattice fringes that can be seen in the HRTEM image in Figure 5g. Note that the lattice spacing in Figure 5f,g is somewhat larger than the observed lattice spacing in the bulk sample as shown in Figure 1e. This is likely caused by the small amount of material that is used in this heating experiment; therefore, allowing the lattice to be expanded. Moreover, the process of cooling down to room temperature is practically instantaneous for such heating experiments (due to its small dimensions and the use of a heating chip instead of an oven), causing the high temperature lattice to be locked in, whereas the slower cooling in the bulk synthesis allows the lattice to equilibrate to a lower temperature. The samples imaged after 6 and 7 weeks, respectively, can be seen in Figure S6, Supporting Information. Unlike the sample from the in situ heating experiment, the samples from the ex-situ experiments remained stable. The transformation of the in situ sample is therefore likely related to the instability of the oxygen-deficient GdO phase, known to have limited stability under both aerial and moist conditions.[29]

In comparison to the bulk synthesis, the small-scale heating experiments require a higher temperature to obtain the same result. This discrepancy can be explained by the overall amount of sample. The large amount of material that is being heated in the bulk combustion synthesis allows the temperature of the material to increase abruptly during the highly exothermic redox reaction. On the small scale of these heating experiments, the higher dissipation of reaction energy inhibits the temperature increase during the reaction. This leaves the question whether combustion took place in the small-scale heating experiments, or if the observed phenomena were only mere decomposition of the starting compounds. According to the literature, the expected formation of Gd_2O_3 during the decomposition of $Gd(NO_3)_3 \cdot 6H_2O$ is between 550 °C and 700 °C under He atmosphere.[30] To investigate this further, a 1.4 mM solution of $Gd(NO_3)_3 \cdot 6H_2O$ in ethanol is drop-casted on a heating chip and heated in situ to 900 °C with 100 °C increments. This sample also shows porosity from 100 °C (Figure S7, Supporting Information), which is attributed to the evaporation of the water that is contained in the gadolinium nitrate. An overview of one of the windows and a corresponding DP can be seen in Figures 5d and d' respectively. Note that the DP is taken at 900 °C; and therefore, displays a larger lattice than the other DPs taken at room-temperature. Although some porosity is present after heating to 900 °C, it is less than seen in the heating experiments of the gel. This becomes clear, especially

from the HRTEM images, where the characteristic 2 to 20 nm large pores are absent; see Figure S7, Supporting Information. Although the absence of glycine in this experiment reduces the amount of gas that is created compared to a possible decomposition of the complete gel, it is more likely that there is indeed a small-scale combustion-like reaction taking place in the heating experiments of the complete gel. This hypothesis is further supported by the fact that this reaction is highly exothermic; and therefore, more favorable. A more extensive study of the reaction mechanism for the glycine-nitrate process is needed to better understand the reaction, which we are currently working on and will be published separately.

3. Conclusion

Highly porous crystalline gadolinium oxide was successfully synthesized, without the use of a template, by combustion synthesis of a gel consisting of gadolinium nitrate and glycine. The surface area and pore size distribution of the material were assessed by nitrogen physisorption. The S_{BET} of the material was determined to be 67 m^2 g^{-1} and the pore size distribution shows the presence of pores in three size ranges. Furthermore, a 3D reconstruction of the nanoporous structure was made using ET employing the weighted back projection algorithm, of which cross-sections revealed the internal nanostructural details of the material. The combustion synthesized Gd_2O_3 had an intricate interconnected pore network consisting of spherical pores with a size ranges varying from 2 to 3 nm to tens of nanometers. The nitrogen physisorption results and the ET results were found to be in good agreement. In addition, small-scale heating experiments of the gel were conducted to further investigate the combustion mechanism of pore formation. The small-scale heating experiments showed a different porosity of the material in comparison to that of the bulk combustion material. Moreover, a higher temperature is needed to form Gd_2O_3 in the small-scale heating experiments, which is probably due to fast cooling of the material on this scale. The decomposition of the gadolinium nitrate precursor indicates that a combustion reaction is happening as well in the small-scale heating experiments, rather than just a decomposition of the gel components. The results indicate that the porosity of the material can be tuned by controlling the experimental conditions during the combustion reaction, such as the scale of the synthesis and the atmosphere in which the gel is heated. In conclusion, gel-combustion synthesis has a great potential to yield crystalline gadolinium oxide nanofoams with a wide range of nanoporous structures that still need to be mapped out.

4. Experimental Section

Combustion Synthesis: A viscous gel containing $Gd(NO_3)_3{\cdot}6H_2O$ and glycine in a 1:1 molar ratio was prepared by dissolving the components in water and drying the solution at 120 °C. Some of the gel was then calcinated in an oven heated to 600 °C with a ramping rate of 20 °C min for 1 h, after which a white powder was obtained.

Physisorption: The specific surface area (S_{BET}) and pore size distribution of the sample were determined by N_2 physisorption at 77 K using a Micromeritics TriStar II Plus. Prior to measuring, the sample was dried for at least 12 h at 300 °C under N_2 flow. The S_{BET} was determined using the Brunauer, Emmett, and Teller (BET) method in the pressure range between 0.04 and 0.2 P/P^o,[31] and the pore size distribution was determined using the BJH method.[32]

In Situ TEM: All TEM investigations were carried out using a TFS Talos F200X electron microscope. For the heating experiments, the gadolinium precursor gel was carefully applied to a DENSsolutions MEMS heating chip, making sure to deposit only a thin layer of gel. In some cases, the gel was diluted with water to make it less viscous. The chip was then inserted in the DENSsolutions heating holder. For the in situ experiment, the gel was inserted into the TEM and heated with 100 °C increments, where it was imaged at every temperature. For the ex situ experiment where the gel was heated to 600 °C, 100 °C increments were also used in order to compare with the in situ experiment. For the ex situ experiment where the gel was heated up to 900 °C, a ramping rate of 20 °C min^{-1} was used in accordance with the bulk gel-combustion synthesis. The exact heating profiles can be seen in Figure S8, Supporting Information.

Electron Tomography: The tilt series were recorded on the same microscope using a tomography holder, where the sample was tilted with 1° increments. The grids were decorated with gold nanoparticles to serve as markers, which later turned out to be unnecessary due to the high contrast of the heavy gadolinium. The tomographic reconstructions were made with Tomviz (www.tomviz.org). The 2048 × 2048 pixel images were first binned to 512 × 512 pixel images. The images were then aligned by cross-correlation, and the tilt axis was aligned by first applying an automatic rotation alignment and then an automatic shift alignment. After aligning the images, the images were cropped to contain only the region of interest. Last, the reconstruction was made using the WBP algorithm,[33] where the Fourier weighting filter was set to ramp and the projection interpolation method to cubic. After reconstruction, the material was segmented by applying a threshold. The surface was smoothed by applying Gaussian blurring with a sigma value of 2.0 and the volume was sliced to make a cross-section. The final visualizations included both the volume and the contours of the segmented areas.

Supporting Information

Supporting Information is available from the Wiley Online Library or from the author.

Acknowledgements

The authors thank Remco Dalebout and Prof. Dr. Petra E. de Jongh from the Materials Chemistry and Catalysis (MCC) group of Utrecht University for performing and facilitating the physisorption measurement. The authors thank Ali Kosari, Hans Meeldijk, and Chris Schneijdenberg from the Electron Microscopy Center of Utrecht University for assistance with the electron microscopy measurements. This research was partly funded by project No. CZ.02.1.01/0.0/0.0/17_049/0008441 "Innovative therapeutic methods of musculoskeletal system in accident surgery" within the "Research and Development for Innovations" Operational Programme financed by the European Union and by Institutional support from the Ministry of Health Czech Republic.

Conflict of Interest

The authors declare no conflict of interest.

Author Contributions

Assisted in the electron microscopy measurements, processed and analyzed the data, and wrote the first version of the manuscript: R.M.d.B. Assisted in the heating experiments: X.C. Provided the samples and

information on the synthesis method: D.C. and K.P.D. Supervised the project and performed the TEM imaging and tomography: R.G.M. Co-supervised the project: M.A.v.H. All authors discussed the results and commented on the manuscript.

Data Availability Statement

The data that support the findings of this study are available from the corresponding author upon reasonable request.

Keywords

electron tomography, gadolinium oxide, in situ TEM, nanofoam

Received: February 20, 2023
Published online: March 31, 2023

[1] B. C. Tappan, S. A. Steiner Iii, E. P. Luther, B. C. Tappan, S. A. S. Iii, E. P. Luther, *Angew. Chem., Int. Ed.* **2010**, *49*, 4544.
[2] G. De Stasio, P. Casalbore, R. Pallini, B. Gilbert, F. Sanità, M. T. Ciotti, G. Rosi, A. Festinesi, L. M. Larocca, A. Rinelli, D. Perret, D. W. Mogk, P. Perfetti, M. P. Mehta, D. Mercanti, *Cancer Res.* **2001**, *61*, 4272.
[3] E. H. Uguru, S. F. A. Sani, M. U. Khandaker, M. H. Rabir, J. A. Karim, *Nucl. Eng. Technol.* **2020**, *52*, 1099.
[4] M. Zinkevich, *Prog. Mater. Sci.* **2007**, *52*, 597.
[5] S. Chaudhary, S. Kumar, S. Kumar, G. R. Chaudhary, S. K. Mehta, A. Umar, *Coatings* **2019**, *9*, 633.
[6] M. M. Abdullah, M. M. Rahman, H. Bouzid, M. Faisal, S. B. Khan, S. A. Al-Sayari, A. A. Ismail, *J. Rare Earths* **2015**, *33*, 214.
[7] M. Shi, Y. Yan, Y. Wei, Y. Zou, Q. Deng, J. Wang, R. Yang, Y. Xu, T. Han, *Int. J. Energy Res.* **2019**, *43*, 6561.
[8] A. Zheng, R. Liang, H. Wu, G. Jiang, M. Fan, J. Xiong, S. Yuan, *Int. J. Electrochem. Sci.* **2022**, *17*, 2.
[9] C. Xu, Y. Chen, W. Zhang, G. Hu, R. Liu, *ACS Appl. Nano Mater.* **2021**, *4*, 1104.
[10] Y. W. He, Q. Wang, X. Yan, L. Q. He, G. Q. Zhang, X. L. Li, *Fullerenes, Nanotubes, Carbon Nanostruct.* **2019**, *27*, 478.
[11] S. Lee, L. P. Lingamdinne, J. K. Yang, Y. Y. Chang, J. R. Koduru, *J. Water Process Eng.* **2021**, *41*, 102083.
[12] R. K. Tamrakar, D. P. Bisen, N. Brahme, *J. Radiat. Res. Appl. Sci.* **2014**, *7*, 550.
[13] V. V. Bakovets, L. N. Trushnikova, P. E. Plyusnin, I. V. Korolkov, I. P. Dolgovesova, T. D. Pivovarova, S. A. Savintseva, *Russ. J. Gen. Chem.* **2013**, *83*, 1808.
[14] S. I. Niftaliev, I. V. Kuznetsova, I. A. Saranov, T. V. Zhundrikova, L. V. Lygina, V. Y. Tuneekov, I. V. Chislova, I. A. Zvereva, *Glass Phys. Chem.* **2019**, *45*, 232.
[15] S. Hazarika, D. Mohanta, *J. Rare Earths* **2016**, *34*, 158.
[16] J. G. Kang, B. K. Min, Y. Sohn, *Ceram. Int.* **2015**, *41*, 1243.
[17] K. Dědková, Kuzníková, L. P. , K. Matějová, J. Kupková, K. Č. Barabaszová, R. Váňa, J. Burda, J. Vlček, D. Cvejn, J. Kukutschová, *Mater. Chem. Phys.* **2017**, *197*, 226.
[18] A. Varma, A. S. Mukasyan, A. S. Rogachev, K. V. Manukyan, *Chem. Rev.* **2016**, *116*, 14493.
[19] W. Wen, J. M. Wu, *RSC Adv.* **2014**, *4*, 58090.
[20] W. Kang, D. O. Ozgur, A. Varma, *ACS Appl. Nano Mater.* **2018**, *1*, 675.
[21] H. Ahmadian, F. Al Hessari, A. M. Arabi, *Ceram. Int.* **2019**, *45*, 18778.
[22] S. Patil, H. P. Dasari, *Mater. Sci. Energy Technol.* **2019**, *2*, 485.
[23] Q. Chen, Y. Shi, J. Chen, J. Shi, *J. Mater. Res.* **2005**, *20*, 1409.
[24] M. Yada, H. Kitamura, A. Ichinose, M. Machida, T. Kijima, *J. Chem. Soc. Perkin Trans. 1* **1999**, *38*, 3506.
[25] D. M. Lyons, L. P. Harman, M. A. Morris, *J. Mater. Chem.* **2004**, *14*, 1976.
[26] W. M. Haynes, D. R. Lide, T. J. Bruno, *CRC Handbook of Chemistry and Physics*, CRC Press, Boca Raton, FL **2014**.
[27] M. Thommes, K. Kaneko, A. V. Neimark, J. P. Olivier, F. Rodriguez-Reinoso, J. Rouquerol, K. S. W. Sing, *Pure Appl. Chem.* **2015**, *87*, 1051.
[28] P. Gilbert, *J. Theor. Biol.* **1972**, *36*, 105.
[29] E. Murad, D. L. Hildenbrand, *J. Chem. Phys.* **1980**, *73*, 4005.
[30] T. Fukuda, Y. Nakano, K. Takeshita, *J. Nucl. Sci. Technol.* **2018**, *55*, 1193.
[31] S. Brunauer, P. H. Emmett, E. Teller, *J. Am. Chem. Soc.* **1938**, *60*, 309.
[32] E. P. Barrett, L. G. Joyner, P. P. Halenda, *J. Am. Chem. Soc.* **1951**, *73*, 373.
[33] M. Radermacher, in *Electron Tomography: Methods for Three-Dimensional Visualization of Structures in the Cell* (Ed.: J. Frank), Springer, New York, NY **2006**, p. 245.